Materials & Design 261 (2026) 115329

Contents lists available at ScienceDirect

Materials & Design

journal homepage: www.elsevier.com/locate/matdes

Ion milling-enhanced preferential growth of $CoSn_3$ for crystallographic orientation control of Sn on polycrystalline Co substrates

Xinjie Wang [a,b,*], Hiroaki Tatsumi [b,*], Chia-Lin Li [c], Jyh-Wei Lee [c,d,e,f], Hiroshi Nishikawa [b]

[a] Graduate School of Engineering, The University of Osaka, Suita 565-0871 Osaka, Japan
[b] Joining and Welding Research Institute, The University of Osaka, Ibaraki 567-0047 Osaka, Japan
[c] Center for Plasma and Thin Film Technologies, Ming Chi University of Technology, New Taipei, Taiwan
[d] Department of Materials Engineering, Ming Chi University of Technology, New Taipei, Taiwan
[e] College of Engineering, Chang Gung University, Taoyuan, Taiwan
[f] High Entropy Materials Center, National Tsing Hua University, Hsinchu, Taiwan

ARTICLE INFO

Keywords:
Orientation relationship
Intermetallic compounds
EBSD
Interface
Edge-to-edge matching

ABSTRACT

Controlling the grain orientation of Sn is vital for enhancing the electromigration reliability of solder joints, particularly in fine-pitch applications where joints may consist of a single grain. In this study, we investigate the use of preferentially grown α-$CoSn_3$ to influence Sn orientation. Firstly, α-$CoSn_3$ formed at the Sn/Co interface during reflow at 267 °C exhibited orientation-dependent growth. Its texture was improved via ion milling, which selectively removed smaller, misoriented grains and preserved well-anchored, favorably oriented ones. This treatment significantly improved the overall crystallographic alignment, with the (600) planes of α-$CoSn_3$ oriented nearly perpendicular to the substrate and the (002) planes parallel to the substrate. Subsequently, Sn powders were melted and solidified on the textured α-$CoSn_3$ surface to induce a preferential orientation, guided by lattice matching. A modified edge-to-edge lattice matching model, predicted the (1 0 1) β-Sn/(600) α-$CoSn_3$ with [0 1 0] β-Sn/[0 1 0] α-$CoSn_3$ as the favorable pairs. EBSD analysis confirmed this prediction, indicating that the [0 0 1] axes of the Sn grains nucleated on ion-milled α-$CoSn_3$ were oriented mostly within 30° of the substrate plane. These results demonstrate that the ion-milled α-$CoSn_3$ surface enables effective Sn orientation control, offering a practical route for improving solder joint reliability.

1. Introduction

The packaging density of electronic components has significantly increased owing to the continuing miniaturization of electronic products, which, in turn, has resulted in a reduction in the size of solder joints [1,2]. Common Pb-free solders typically contain over 95 % Sn [3]. When the joint size is reduced below 100 μm, each solder joint often consists of a single nucleation event, resulting in either a single Sn grain or cyclic twin structure [4,5].

Sn exhibits pronounced anisotropy owing to its unique tetragonal crystal structure. The coefficient of thermal expansion and Young's modulus along the c-axis are approximately two and three times those along the a/b axes, respectively [6,7]. Moreover, the diffusion coefficients of common solutes (Cu [8], Ag [9], and Ni [10]) along the c-axis are significantly higher than those along the a/b axes. Thus, the reliability of solder joints depends strongly on the orientation of Sn grains [11]. When the c-axis of Sn is aligned parallel to the direction of the current, the joint suffers more severe electromigration-induced damage [12–14]. This typically manifests as substrate depletion at the cathode side and excessive intermetallic compounds (IMCs) precipitation at the anode side, shortening the lifetime of the solder joint [11]. In contrast, when the c-axis is perpendicular to the current flow, electromigration-induced damage is significantly suppressed, leading to improved reliability [15]. Owing to the increased current density in miniaturized joints, addressing electromigration reliability is increasingly urgent, with the Sn grain orientation being a critical factor [16,17].

Thus, effectively controlling the Sn grain orientation in solder joints is a crucial challenge. Z.L. Ma et al. innovatively demonstrated that several IMCs ($PtSn_4$, $CoSn_3$, and $IrSn_4$) possess crystal structures similar to that of Sn [5,18]. For the representative α-$CoSn_3$ IMCs, they proposed orientation relationships (ORs) based on the plane-on-plane model, namely: {100} Sn/{100}$CoSn_3$ with <001>Sn/<001>$CoSn_3$, and {100}Sn/{100}$CoSn_3$ with <001>Sn/<010>$CoSn_3$. Therefore, these IMCs can serve as seed

* Corresponding authors.

https://doi.org/10.1016/j.matdes.2025.115329
Received 4 September 2025; Received in revised form 5 December 2025; Accepted 11 December 2025
Available online 11 December 2025

crystals to control Sn orientation during solidification. However, this approach requires additional processing steps, such as bonding seed crystals to the substrate prior to solder ball placement, and the high cost of single-crystal seeds limits its industrial feasibility. Nevertheless, this pioneering work creatively utilized lattice matching to control Sn grain orientation in solder joints, provided valuable inspiration for subsequent research. Another strategy involves the use of single-crystal Co substrates to form orientation-defined $CoSn_3$, which, in turn, can control Sn orientation [19]. For example, Sn nucleated on $(10\bar{1}0)$ Co tends to avoid aligning its c-axis parallel to the direction of current flow, thereby potentially enhancing electromigration resistance. However, the high cost of single-crystal Co substrates similarly hinders industrial adoption.

Improving upon these existing approaches to achieve effective control of Sn grain orientation remains a critical challenge. Motivated by this, we considered whether a processing strategy could be applied to conventional polycrystalline Co substrates to enhance the preferred orientation of Co–Sn IMCs formed at the interface, thereby improving the feasibility of Sn orientation control. We referred to industrial techniques known to strengthen crystallographic texture. According to previous studies, in thin-film post-processing, film texture can be significantly enhanced under ion-beam treatment. Under ion irradiation, grains with specific orientations favorable to channeling effects grow preferentially, while others are suppressed, leading to the development of a strong texture [20,21]. Inspired by these findings, ion-beam processing was introduced in this study to improve the orientation characteristics of Co–Sn IMCs. Compared with the use of single-crystal seeds, the ion-beam method eliminates the need for precise seed transfer and bonding — two highly challenging steps — and instead utilizes the standard Co–Sn interfacial reaction to in situ generate IMCs layers. This is a spontaneous, scalable, and microelectronics-compatible process. Moreover, broad-beam ion irradiation enables uniform treatment of large-area samples, demonstrating potential scalability for industrial production.

The aforementioned studies specifically highlight the metal Co due to its extensive application potential in the electronics manufacturing industry. Co can serve as an effective diffusion barrier layer, suppressing excessive formation of brittle Cu–Sn IMCs while forming ductile Co–Sn IMCs that ensure excellent interfacial bonding strength and mechanical reliability during thermal fatigue testing [22–24]. Furthermore, Co as a new interconnect material for next-generation semiconductor devices, exhibits excellent electromigration resistance [25,26]. Therefore, systematic investigation of interfacial reactions on Co substrates is essential to deepen our understanding of their performance and enable successful implementation.

In this study, we explore the potential of α-$CoSn_3$ IMCs for influencing Sn grain orientation. First, we observed that even on polycrystalline Co, the IMCs formed at the Sn/Co interface exhibit certain preferential growth characteristics. This preferred orientation can be further enhanced via argon ion milling. Subsequently, Sn powders were melted and solidified on the ion-milled α-$CoSn_3$ surfaces. The orientation relationships (ORs) were analyzed using the edge-to-edge matching model, and the predicted β-Sn/α-$CoSn_3$ orientation pairs were validated through electron backscatter diffraction (EBSD) analysis of Sn grains nucleated on ion-milled α-$CoSn_3$ surfaces.

2. Experimental

The experimental procedure can be summarized as follows. First, Sn/Co samples were fabricated through a reflow process to form α-$CoSn_3$ IMCs. Subsequently, excess Sn was chemically removed, followed by ion milling treatment to achieve both a planar IMCs surface and enhanced crystallographic texture. Finally, Sn powders were reflowed on the prepared IMCs surface, and the crystallographic orientation of the nucleated Sn grains was characterized via EBSD.

Fig. 1 shows a schematic of the experimental procedure. As shown in Fig. 1 (a), the Sn/Co samples were prepared by stacking a 100 μm-thick pure Sn foil onto a 5 mm × 5 mm × 1 mm Co substrate (The Nilaco Corporation). A commercial SR-12 flux (Senju Metal Industry Co., Ltd.) was used to remove surface oxides. The commercial reflow furnace (SMT Scope SK-5000, Sanyo Seiko Co., Ltd.) was used for reflow at 267 °C for 10 or 20 min.

Excess Sn after reflow was removed using 10 % HNO_3 to expose the Sn/Co interfacial IMCs, as shown in Fig. 1(b). The morphology and composition of the IMCs were analyzed using a scanning electron microscope (JEOL JSM-IT200). The samples were subsequently subjected to argon ion milling (JEOL IB-19530CP), with the ion beams directed nearly parallel to the substrate surface. Flat IMCs surfaces were obtained after milling at 6 kV for approximately 1 h, as shown in Figs. 1(c) and (d).

The crystallographic orientation of the ion-milled IMCs was characterized via X-ray diffraction (XRD) and electron backscatter diffraction (EBSD). XRD analysis was performed by D8 DISCOVER (Bruker Corporation) with Co Kα radiation in θ/2θ scanning mode. In addition, EBSD measurements were carried out with EDAX-TSL system.

For Sn wetting, 150 μm Sn powders (Kojundo Chemical Laboratory Co., Ltd.) were melted and spread on the ion-milled α-$CoSn_3$ surfaces under reflow at 260 °C for 20 s, as shown in Figs. 1(e) and (f). These samples were then subjected to further ion milling followed by EBSD to analyze the crystallographic orientations of the Sn grains.

3. Prediction of orientation relationships between β-Sn and α-$CoSn_3$ using a modified edge-to-edge model

3.1. Modification of the edge-to-edge model

Current orientation control models frequently employ two approaches based on lattice matching: the plane-on-plane model [27,28] and the edge-to-edge model [29]. Both approaches emphasize the role of close-packed planes and directions. A schematic of these two models is shown in Fig. 2. As the names suggest, the former assumes that the close-packed planes in phase B grow parallel and on top of the planes in phase A. If their planar mismatch is low, matching is feasible. In contrast, the edge-to-edge model is based on the matching of rows of atoms across the interface [29]. In this model, the close-packed planes of phase A and phase B act as intersection planes to form the interface, typically with their close-packed directions aligned at the edge to establish matching directions.

This study based on the phase of β-Sn and α-$CoSn_3$. Specifically, β-Sn has a tetragonal structure with the space group $I4_1/amd$ and lattice parameters (a = 5.831 Å, b = 5.831 Å, and c = 3.181 Å). In contrast, α-$CoSn_3$ exhibits an orthorhombic crystal structure with the space group Cmca and lattice parameters (a = 16.864 Å, b = 6.268 Å, c = 6.270 Å). Considering that α-$CoSn_3$ exhibits a natural preferred orientation with the (600) close-packed plane nearly perpendicular to the substrate surface, ion milling was applied to selectively remove smaller, misoriented grains, thereby exposing the edges of the (600) planes that could subsequently influence Sn nucleation. Given this configuration, the edge-to-edge matching model was primarily employed in this study to predict the crystallographic ORs between β-Sn and α-$CoSn_3$.

The conventional model was modified appropriately to enable a more comprehensive prediction of ORs. Specifically, when analyzing the matching directions between α-$CoSn_3$ and β-Sn, we considered the two distinct atom row configurations: straight and zigzag rows. This means that any close-packed or nearly close-packed atom rows—even those with differing morphologies—can potentially form a matching pair [30]. As shown in Fig. 3(a), favorable matching can occur between straight and zigzag rows under appropriate geometric conditions. Furthermore, we extended our analysis to more complex close-packed directions, such as the [011] direction in α-$CoSn_3$, which incorporates both straight and zigzag row features.

Two critical parameters, namely the effective interatomic spacing and d-value, must be defined before lattice matching calculations. As

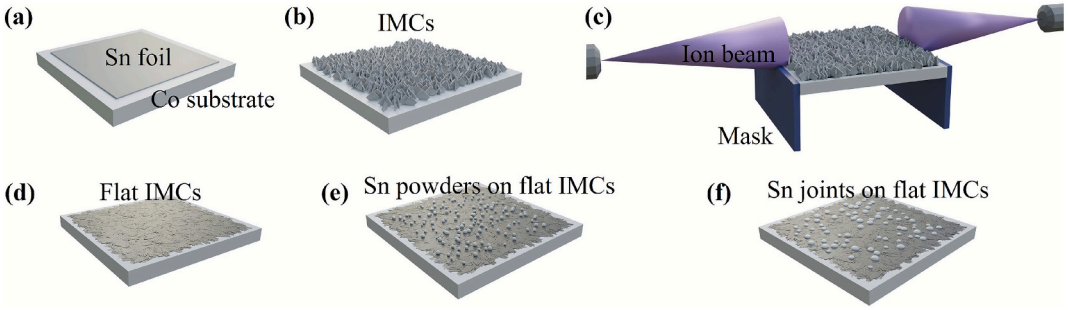

Fig. 1. Schematic of the experimental procedure. (a) Sn foil stacked on polycrystalline Co substrate to form the Sn/Co sample, followed by a reflow experiment. (b) Interfacial IMCs obtained after removing excess Sn from the reflowed Sn/Co sample using 10% HNO_3. (c) Ion milling applied from two directions to the IMCs to enhance their preferred orientation. (d) Flat IMCs surface achieved after ion milling. (e) Sn powders placed on the ion-milled IMCs, followed by reflow to form the Sn joints in (f).

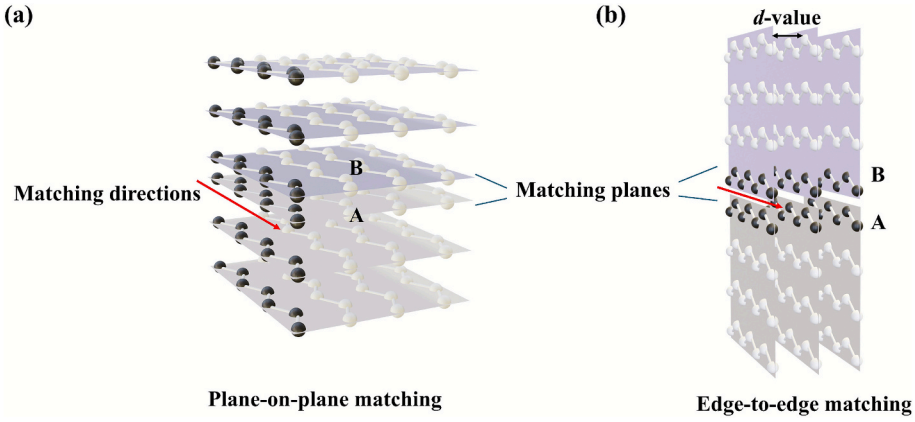

Fig. 2. Schematic of the plane-on-plane and edge-to-edge matching approaches. (a) The plane-on-plane model, where the close-packed planes of phase A and phase B are nearly parallel and stacked at the interface, with their close-packed directions aligned to form matching directions. (b) The edge-to-edge model, in which the close-packed planes of phase A and phase B act as intersection planes to form the interface, typically with their close-packed directions aligned at the edge to establish matching directions.

shown in Fig. 3 (b), the effective interatomic spacing refers to the projected distance between adjacent atoms along the matching directions. Atom rows in these directions typically exhibit two distinct configurations: straight and zigzag rows. The effective interatomic spacing for zigzag rows corresponds to the projected atomic spacing onto a straight line, as shown in Fig. 3 (b, c1, and c2). In α-$CoSn_3$, the [0 1 1] atom row exhibits a more complex structure, incorporating both straight and zigzag features. In such cases, the average atomic spacing along this direction is used to define the effective interatomic spacing. The d-value represents the interplanar spacing between close-packed planes in the crystal structure, as shown in Fig. 3 (d1 and d2).

3.2. *Prediction of the orientation relationships between β-Sn and α-$CoSn_3$*

3.2.1. *Identification of the matching directions*

The conventional edge-to-edge model was generally followed for predicting the ORs between β-Sn and α-$CoSn_3$. In this approach, the close-packed or nearly close-packed directions in both phases must first be identified to serve as the matching directions. The computational procedure necessitates the incorporation of specific crystallographic information [31,32]. The effective interatomic spacing was then calculated by considering the atomic coordinates, ultimately yielding the close-packed or nearly close-packed directions. The computational results are summarized in Table 1.

The mismatch between β-Sn and α-$CoSn_3$ was evaluated using the formula: $(f_\beta - f_\alpha)/f_\alpha$, where f_β and f_α denote the effective interatomic spacings for β-Sn and α-$CoSn_3$, respectively. Direction pairs with mismatch values below 10 % were considered valid [33], as summarized in Table 2.

3.2.2. *Identification of matching planes*

The subsequent step involves identifying the close-packed or nearly close-packed planes in both β-Sn and α-$CoSn_3$ as the matching planes. These matching planes must incorporate the matching directions calculated in the preceding section. The Powder Diffraction File (ICDD Card No. 00–048-1813 and 01–086-2264) were consulted to identify the high-intensity diffraction planes, which typically correspond to close-packed or nearly close-packed planes [31,32]. Subsequently, the d-values of the identified planes were carefully evaluated. The corresponding planes should generally have a less than 6 % d-value mismatch to qualify as valid matching planes [33]. The calculated d-values and their corresponding mismatch percentages for β-Sn and α-$CoSn_3$ are presented in Tables 3 and 4.

In lattice matching theory, the OR between two phases is determined by combining the matching directions and matching planes. Thus, we integrated the computed direction-matching and plane-matching pairs to deduce possible ORs between β-Sn and α-$CoSn_3$ (Table 5). The lattice matching results were plotted to visualize these relationships and are shown in Fig. 4. All ORs were categorized into two groups based on close-packed plane matching: (200) β-Sn/(600) α-$CoSn_3$ and (1 0 1) β-Sn/(600) α-$CoSn_3$. Subsequently, we conducted a series of experiments to verify whether the predicted ORs exist between β-Sn and α-$CoSn_3$.

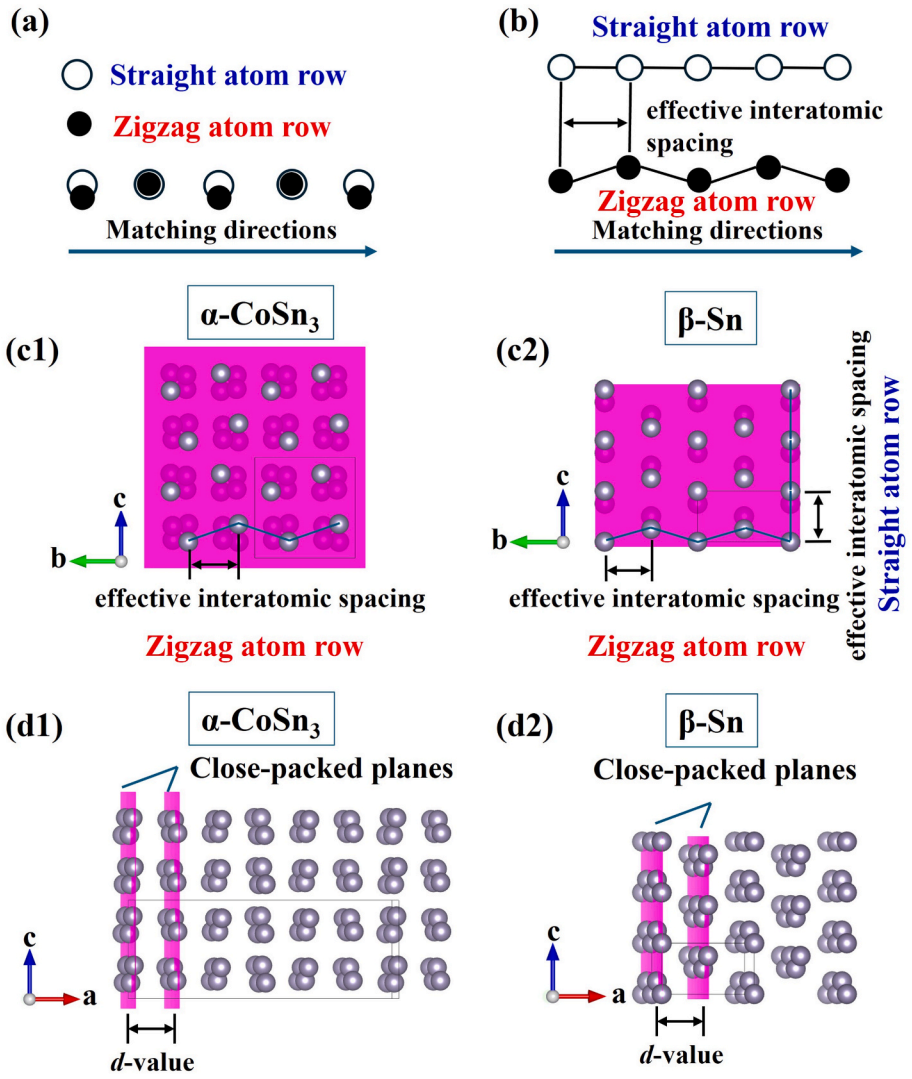

Fig. 3. Schematic of the effective interatomic spacing and d-values. (a) Atom matching between straight and zigzag atom rows. (b) Effective interatomic spacing for straight and zigzag atom rows. (c1, c2) Effective interatomic spacing for α-$CoSn_3$ and β-Sn. (d1, d2) d-values for α-$CoSn_3$ and β-Sn.

Table 1
Effective interatomic spacing for the close-packed directions in β-Sn and α-$CoSn_3$.

Phase	Close-packed directions	Effective interatomic spacing (Å)
β-Sn	[100]	2.916
	[010]	2.916
	[001]	3.181
	[011]	3.321
	[101]	3.321
α-$CoSn_3$	[010]	3.134
	[001]	3.135
	[011]	2.955

Table 2
Interatomic spacing mismatch (%) along potential alignment directions between β-Sn and α-$CoSn_3$.

Matching directions		Interatomic spacing mismatch (%)
β-Sn	α-$CoSn_3$	
[100]/[010]	[001]	6.99
	[010]	6.96
	[011]	1.32
[001]	[001]	1.47
	[010]	1.50
	[011]	7.65
[011]/[101]	[001]	5.93
	[010]	5.97

4. Results and discussion

4.1. Morphology and composition of the as-formed IMCs

As shown in Fig. 5, the IMCs formed at the Sn/Co interface exhibited a plate-like morphology. With an increase in the reflow time from 10 to 20 min, these plate-shaped IMCs tended to merge along their largest facets to form thicker bulk structures. After 10 min of reflow, the tip directions of the plates were randomly distributed, whereas after 20 min, most IMCs grew with their sharp tips aligned nearly perpendicular to the substrate. These results suggest that under prolonged reflow, IMCs with faster growth orientations tend to outgrow or consume their slower-growing counterparts.

Elemental analysis using energy-dispersive X-ray spectroscopy (EDS) was conducted at three different positions to ensure representative results. Based on the compositional analysis results shown in Fig. 6, the IMCs were confirmed to be $CoSn_3$. Previous studies have reported that $CoSn_3$ exhibits strong growth anisotropy, with rapid growth occurring along directions corresponding to the plate corners and relatively slow

Table 3
D-values for the close-packed planes in β-sn and α-$CoSn_3$.

Phase	Close-packed planes	d-values (Å)
β-Sn	(200)	2.915
	(101)	2.793
	(211)	2.017
α-$CoSn_3$	(002)	3.135
	(600)	2.811
	(221)	2.659
	(312)	2.511
	(022)	2.217
	(113)	1.969

Table 4
D-value mismatch (%) of possible plane pairs between β-sn and α-$CoSn_3$.

Matching planes β-Sn	α-$CoSn_3$	d-value mismatch (%)
(200)	(600)	3.70
(101)	(600)	0.64
(101)	(221)	5.04
(211)	(113)	2.44

growth along close-packed planes, leading to the formation of well-defined facets [34,35].

4.2. Crystallographic orientation of the ion-milled IMCs

As described earlier, after 20 min of reflow, the $CoSn_3$ crystals exhibited more pronounced orientation features, with most plate-shaped IMCs growing nearly perpendicular to the substrate. Their crystallographic characteristics were verified by subjecting them to argon ion milling to expose planes perpendicular to the fast-growth directions, as shown in Fig. 7.

Smaller IMCs, which are often misaligned or loosely attached, are readily removed by argon ion milling owing to their weak contact with the substrate. In contrast, larger grains with preferred orientations remain anchored firmly at the interface. Thus, the flat surface exposed by ion milling reflects primarily the dominant orientation of the well-oriented $CoSn_3$ grains.

Fig. 8 shows the XRD patterns of the IMCs before and after ion milling. The intensity of the (600) plane decreased with an increase in the reflow time (from 10 to 20 min), possibly because of the merging of the plate-like IMCs and a reduction in the exposure of the (600) facets. After ion milling, the intensity of the (002) peak increased significantly and was the highest, followed by the intensity of the (113) peak.

The XRD pattern reflects both crystallographic packing and texture. Although the Powder Diffraction File (ICDD Card No. 00–048-1813) indicates that the (312) plane exhibits the highest intensity, this peak was largely absent in the reflowed and ion-milled sample. According to Leineweber et al., the diffuse hump near the (312) peak can be attributed to stacking disorder in $CoSn_3$ [36]. Nonetheless, the significantly enhanced intensity ratio of the (002) peak after extended reflow and ion milling suggests that the sample developed a (002) preferred orientation.

The relatively strong (113) intensity may be due to two factors: its close-packed nature and the small angle between (002) and (113). As shown in Fig. 8(b), when the IMCs grow preferentially along the direction perpendicular to (002), a slight tilt can result in (113) aligning parallel to the substrate and thereby, exposed after ion milling.

Table 5
Possible matching directions and the corresponding matching planes between β-Sn and α-$CoSn_3$.

Orientation relationship	Matching directions on the edge	Matching planes
A1	$[001]_{\beta\text{-Sn}}/[010]_{\alpha\text{-CoSn3}}$	$(200)_{\beta\text{-Sn}}/(600)_{\alpha\text{-CoSn3}}$
A2	$[010]_{\beta\text{-Sn}}/[010]_{\alpha\text{-CoSn3}}$	$(200)_{\beta\text{-Sn}}/(600)_{\alpha\text{-CoSn3}}$
A3	$[011]_{\beta\text{-Sn}}/[010]_{\alpha\text{-CoSn3}}$	$(200)_{\beta\text{-Sn}}/(600)_{\alpha\text{-CoSn3}}$
A4	$[010]_{\beta\text{-Sn}}/[011]_{\alpha\text{-CoSn3}}$	$(200)_{\beta\text{-Sn}}/(600)_{\alpha\text{-CoSn3}}$
A5	$[001]_{\beta\text{-Sn}}/[011]_{\alpha\text{-CoSn3}}$	$(200)_{\beta\text{-Sn}}/(600)_{\alpha\text{-CoSn3}}$
B1	$[010]_{\beta\text{-Sn}}/[010]_{\alpha\text{-CoSn3}}$	$(101)_{\beta\text{-Sn}}/(600)_{\alpha\text{-CoSn3}}$
B2	$[10\bar{1}]_{\beta\text{-Sn}}/[010]_{\alpha\text{-CoSn3}}$	$(101)_{\beta\text{-Sn}}/(600)_{\alpha\text{-CoSn3}}$
B3	$[010]_{\beta\text{-Sn}}/[011]_{\alpha\text{-CoSn3}}$	$(101)_{\beta\text{-Sn}}/(600)_{\alpha\text{-CoSn3}}$

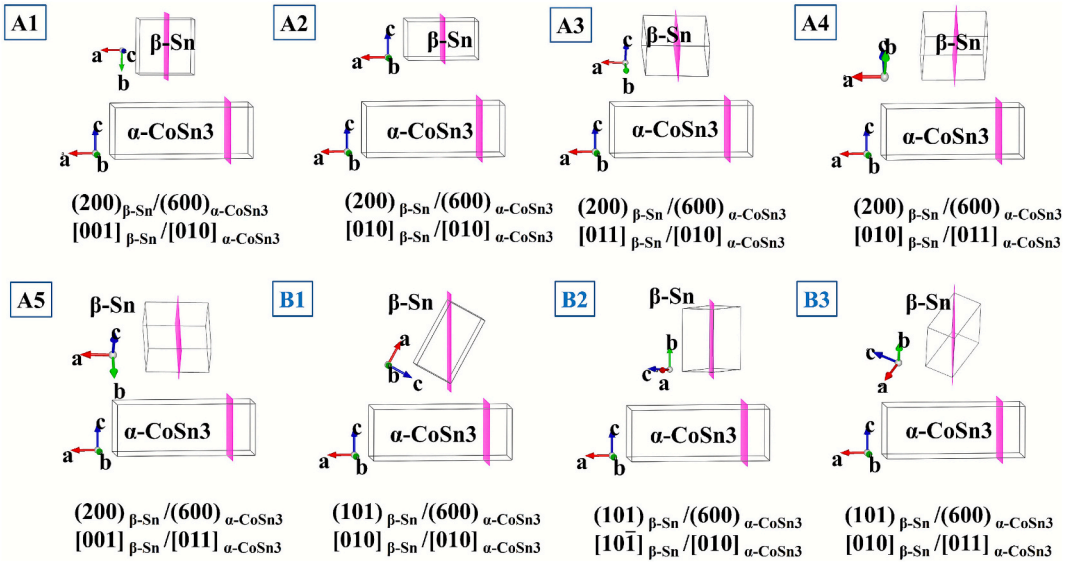

Fig. 4. Schematic of the predicted orientation relationship between β-Sn and α-$CoSn_3$, categorized into groups A and B based on different close-packed planes.

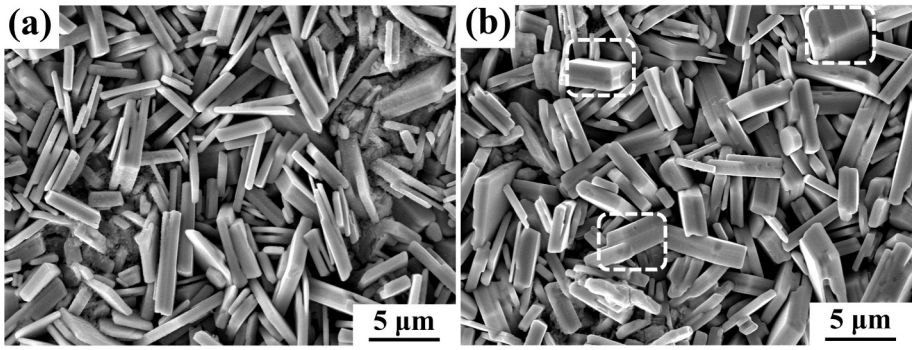

Fig. 5. Top-view morphology of IMCs at the Sn/Co interface for reflow durations of (a) 10 min and (b) 20 min, where residual Sn has been etched away for imaging.

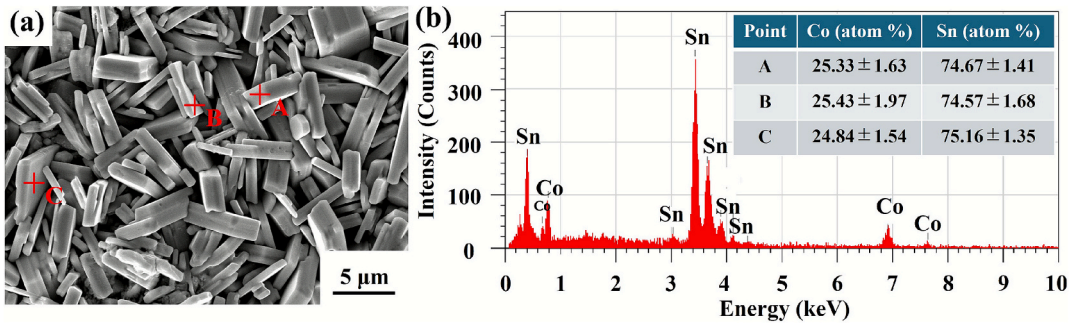

Fig. 6. EDS compositional analysis results of the IMCs at the Sn/Co interface and their corresponding measurement locations.

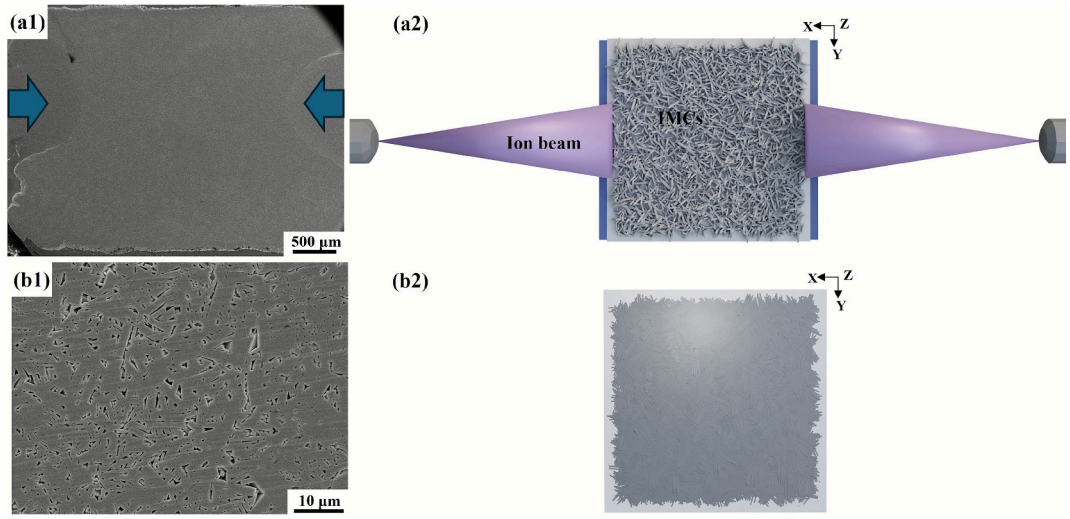

Fig. 7. Schematic of the acquisition of flat IMC surfaces through dual-sided ion milling from directions parallel to the substrate. (a1) Ion milling performed from both sides to obtain a flat IMCs surface, with (a2) showing a schematic of this process. (b1) Surface morphology of ion-milled IMCs at higher magnification. (b2) Schematic of the resulting flat IMCs surface achieved through the dual-sided ion milling treatment described in (a2).

These results were further validated via EBSD. Fig. 9 shows the top-view EBSD maps of the ion-milled IMCs. Most α-$CoSn_3$ grains appeared red or blue in the inverse pole figure, indicating that their (010) or (001) planes were parallel to the substrate. Although α-$CoSn_3$ exhibits an orthorhombic structure, the lengths of the b- and c-axes were nearly identical, rendering the (010) and (001) planes indistinguishable in the EBSD analysis. These EBSD results, combined with the XRD results, confirm that the (001) plane is nearly parallel to the substrate.

The pole figures further supported this observation: high intensity for (010)/(001) was concentrated at the center and periphery, whereas the (100) pole figure exhibited high intensity peaks only around the circumference, indicating that the (100) plane is generally perpendicular to the substrate.

Thus, the XRD and EBSD results confirmed that, even on polycrystalline Co, ion-milled α-$CoSn_3$ exhibits strong preferential growth: the (002) plane is parallel and the (600) plane is perpendicular to the substrate.

It is worth noting that Lang and Jeitschko reported that $CoSn_3$ exists in two polymorphs, with a phase transition from α to β occurring above 275 °C [32]. Although the α and β phases possess different crystal structures—α-$CoSn_3$ being orthorhombic and β-$CoSn_3$ tetragonal—they nevertheless exhibit certain structural similarities. Specifically, α-$CoSn_3$

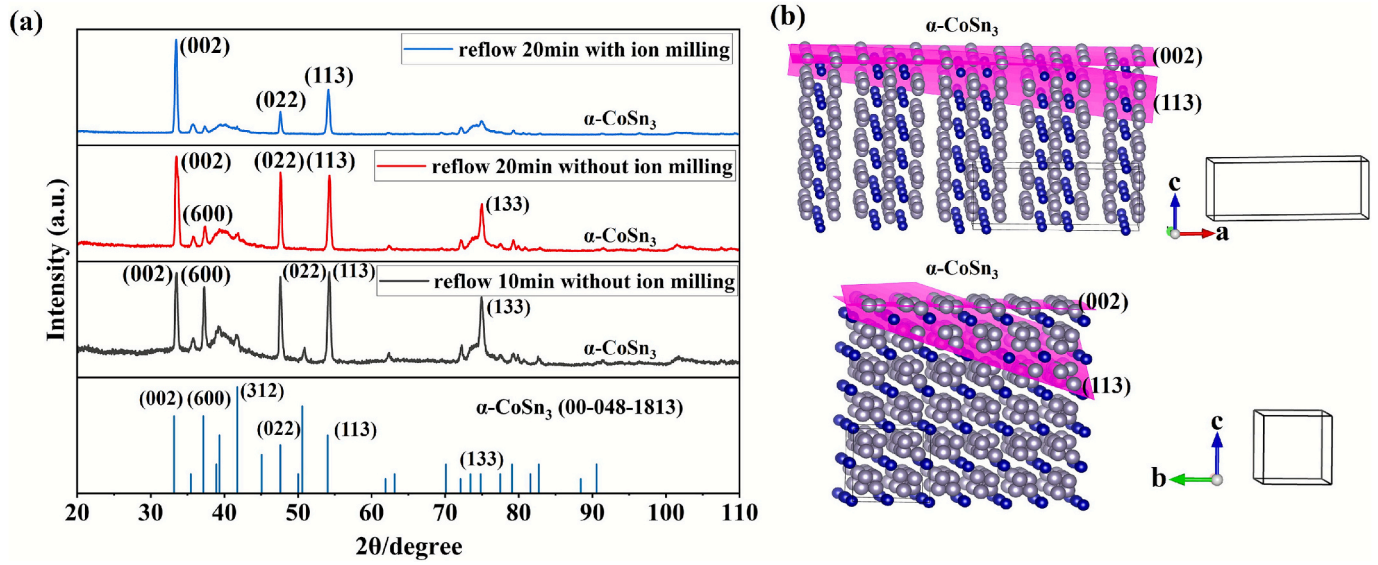

Fig. 8. XRD results and schematic of the crystal planes. (a) XRD analysis of the interfacial IMCs before and after ion milling. (b) Schematic of the (002) and (113) planes in α-$CoSn_3$.

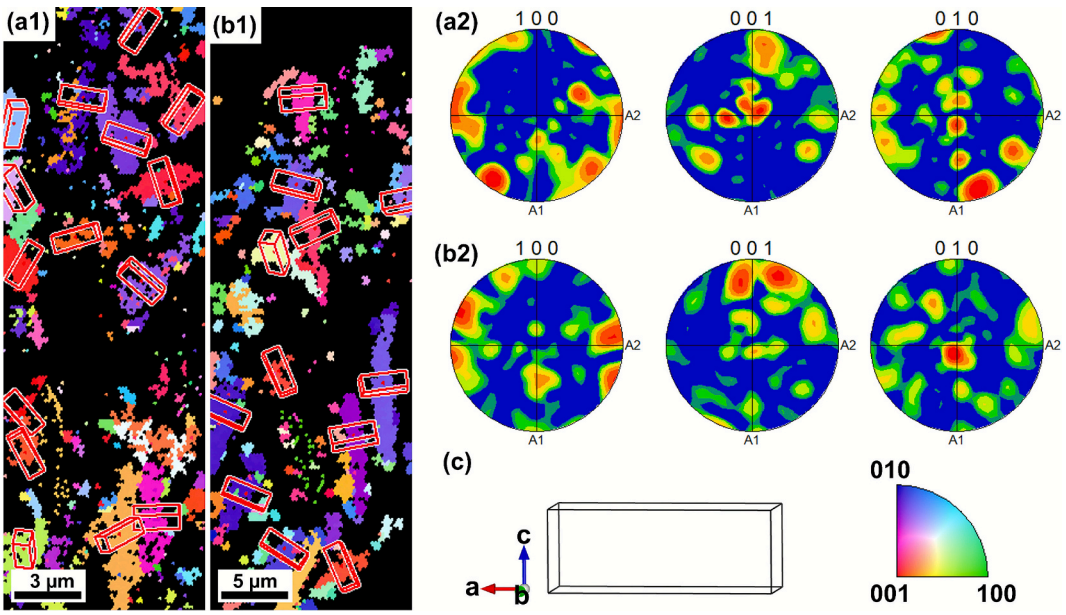

Fig. 9. Top-view EBSD analysis of the ion-milled IMCs with corresponding pole figures. (a1, b1) Top-view EBSD maps. (a2, b2) Corresponding pole figures of (a1, b1). (c) Schematic diagram of the α-$CoSn_3$ structure. The EBSD maps display only the regions with a confidence index higher than 0.25.

(b = 6.268 Å, c = 6.270 Å) and β-$CoSn_3$ (a = 6.275 Å, b = 6.275 Å) show similar lattice parameters, whereas along specific crystallographic directions, the lattice constants of α-$CoSn_3$ (a = 16.864 Å) and β-$CoSn_3$ (c = 33.740 Å) differ by approximately a factor of two. Consequently, when it comes to certain crystal planes, the β-phase Kikuchi pattern exhibits finer band spacing, while corresponding bands in the α-phase pattern tend to merge or vanish. In this study, EBSD indexing was performed for both α and β phases, and the α-phase indexing yielded higher confidence index values. Considering that the interfacial reaction temperature in our experiments was below the α–β transition temperature, the present work focuses on the α-$CoSn_3$ phase throughout the analysis.

4.3. Orientation distribution of the Sn grains formed on ion-milled IMCs

EBSD was used to examine the orientation distribution of the Sn grains nucleated on ion-milled IMCs and validate the predicted ORs between β-Sn and α-$CoSn_3$ and the edge-to-edge model.

Fig. 10 shows the experimental setup and surface morphology of Sn joints: Sn powders melted and solidified on the ion-milled IMCs surface. In some regions, the Sn powders coalesced into larger joints. These joints were ion milled parallel to the substrate surface to enable EBSD analysis.

Fig. 11 shows the grain orientations of Sn joints formed on ion-milled α-$CoSn_3$ IMCs. As observed in Fig. 11(a3, b3, c), most Sn grains appear green, indicating that their (100) planes are nearly parallel or slightly inclined relative to the substrate. Further analysis in Fig. 11(d) shows that the angle between the Sn [001] axis and the substrate plane primarily falls between 15° and 30°, with a pronounced peak near 22.5–30°.

To interpret this, we first recall the ORs reported by Z.L. Ma et al.: {100}Sn/{100}$CoSn_3$ with <001>Sn/<001>$CoSn_3$, and {100}Sn/

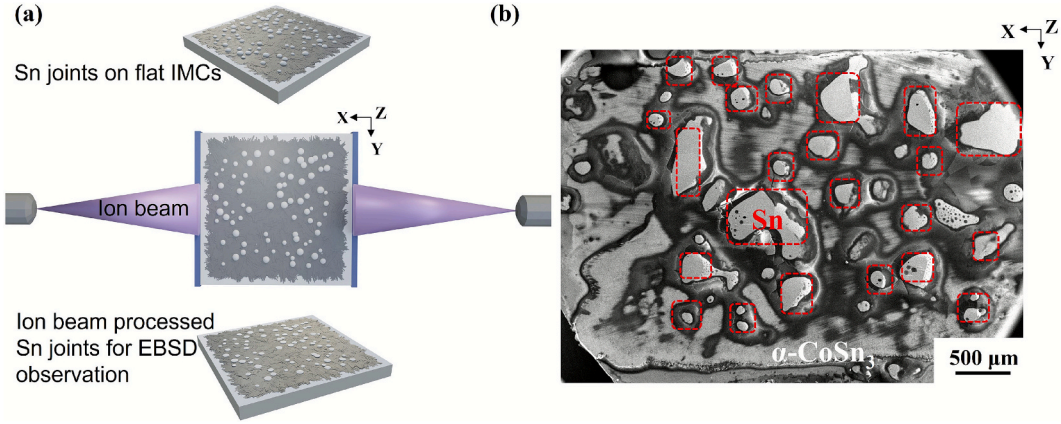

Fig. 10. Experimental setup and surface morphology of Sn joints. (a) Schematic of the Sn joints formed on ion-milled IMCs, followed by additional ion-milling treatment to prepare the joints for subsequent EBSD characterization. (b) Surface morphology of the Sn joints after ion milling.

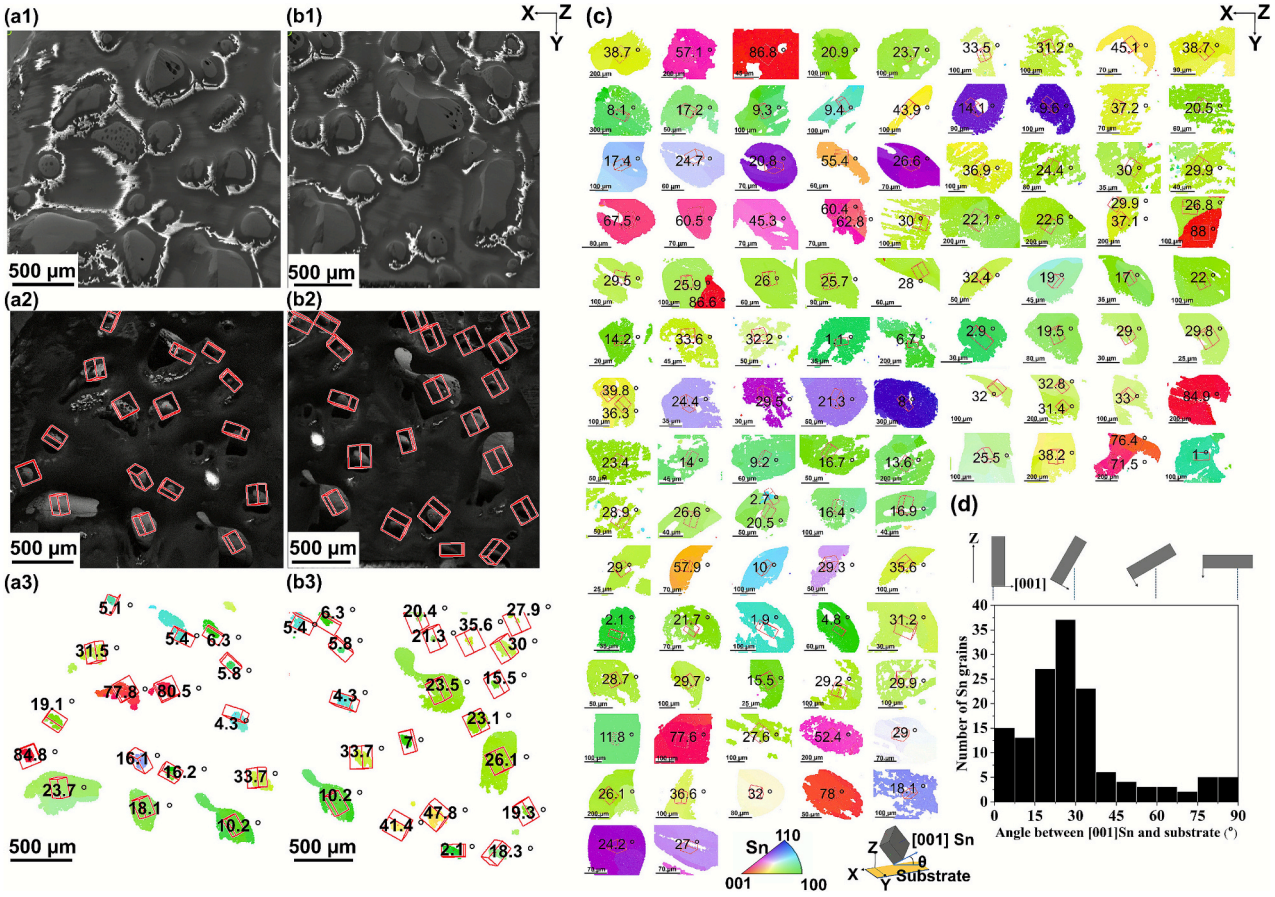

Fig. 11. EBSD maps and grain orientation statistics. (a1, b1) Top-view SEM images showing Sn grains formed on ion-milled IMCs. (a2, b2) Top-view EBSD image quality maps. (a3, b3) Top-view EBSD inverse pole figure maps with Sn grain orientations. (c) Combined top-view EBSD inverse pole figure maps of Sn grain orientations for a large amount of samples. (d) Grain orientation statistics for the Sn grains formed on ion-milled IMCs.

{100}$CoSn_3$ with <001>Sn/<010>$CoSn_3$ [5]. Although α-$CoSn_3$ has an orthorhombic structure, its b and c lattice parameters are nearly identical (b = 6.268 Å, c = 6.270 Å); thus, alignment of Sn <001>with either the b-axis or c-axis of α-$CoSn_3$ occurs with nearly equal probability, resulting in two possible ORs. It is important to note that their study assumed the {100} close-packed planes of α-$CoSn_3$ seeds were parallel to the substrate surface, which promoted epitaxial Sn growth via the plane-on-plane model.

In contrast, in this study, due to the natural growth behavior of α-$CoSn_3$—where the (600) close-packed plane is nearly perpendicular to the substrate—and the subsequent ion milling process that selectively removed misoriented α-$CoSn_3$ grains, the IMCs developed a strong preferred orientation. However, the (600) planes (largest facets of IMCs) were no longer directly exposed but influenced Sn nucleation through their edges. According to Figs. 8 and 9, while the (002) planes of α-$CoSn_3$ are nearly parallel to the substrate and the (600) planes are nearly perpendicular, the geometrically dominant facets corresponding to the (600) planes remain concealed, with only the closely-packed atom rows

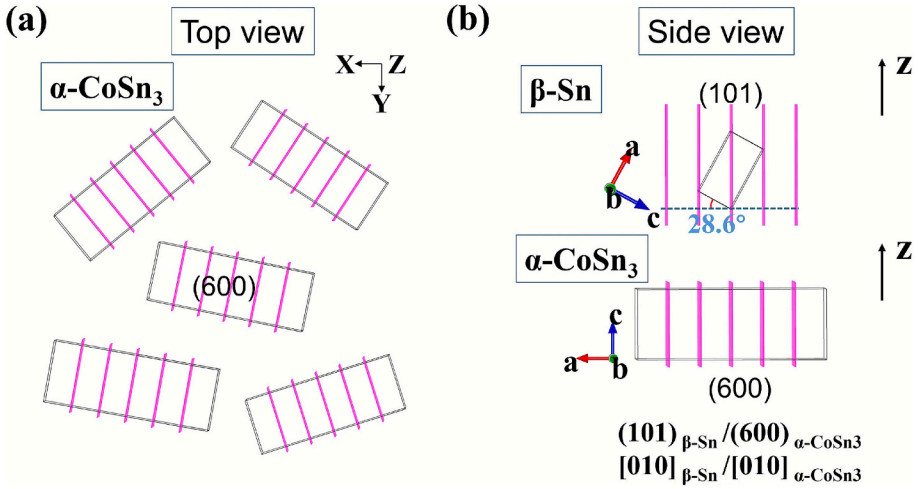

Fig. 12. Schematic of the growth characteristic of α-$CoSn_3$ and the edge-to-edge matching between β-Sn and α-$CoSn_3$. (a) Top-view observation showing the growth characteristic of α-$CoSn_3$ at the Sn/Co interface with close-packed (600) planes nearly perpendicular to the substrate. (b) Side-view illustration of the edge-to-edge matching orientation relationship between (101) β-Sn and (600) α-$CoSn_3$, along with the angle between the Sn [001] axis and the substrate plane.

at their edges being exposed. If we followed the plane-on-plane model of Z.L. Ma et al, Sn grains nucleated on ion-milled α-$CoSn_3$ should exhibit orientations corresponding to cases A1 and A2 in Table S1, meaning the Sn [001] axis would align at 0° or 90° relative to the substrate, with nearly equal probabilities. However, our experimental data show angles concentrated between 15°–30°, with a clear peak at 22.5°–30°. This observation can be explained using Fig. 12: for the configuration (101) β-Sn/(600) α-$CoSn_3$ with [010] β-Sn/[010] α-$CoSn_3$, the angle between the Sn [001] axis and the substrate is 28.6°, matching the observed resluts.

This OR may be attributed to a low interfacial energy, which energetically favors nucleation. According to the classical framework of nucleation theory and its extension by Turnbull [37–39], the nucleation barrier ΔG^* at the interface is proportional to the cube of the interfacial energy (γ_{int}):

$$\Delta G^* \propto \frac{{\gamma_{int}}^3}{(\Delta G_v)^2}$$

Where ΔG^* denotes the nucleation barrier, γ_{int} is the interfacial energy, and ΔG_v is the volumetric free energy change. γ_{int} is minimized when the lattice mismatch and orientation discontinuity are small. The (1 0 1) β-Sn/(600) α-$CoSn_3$ configuration showed the lowest d-value mismatch (0.64 %). Therefore, Sn grains with their (1 0 1) planes aligned with the (600) planes of α-$CoSn_3$ experience significantly reduced nucleation barriers.

Furthermore, the [001] direction in β-Sn corresponds to the c-axis, which is both the fast diffusion path and the direction corresponding to the highest electromigration vulnerability. By promoting orientations wherein [001] is tilted away from the vertical current flow (i.e., substrate normal), this interface-induced texture can reduce the effective diffusivity under current stress, thereby enhancing electromigration resistance.

In summary, the present study demonstrates that after ion milling, α-$CoSn_3$ IMCs expose only the edges of their close-packed (600) planes, which also effectively guide Sn nucleation. The experimental results shown in Fig. 11 confirm that the modified edge-to-edge model successfully predicts the ORs of Sn grains nucleated on ion-milled α-$CoSn_3$. Meanwhile, comparative experiments using α-$CoSn_3$ IMCs without ion milling (Fig. S1) show that Sn [001] axes are more randomly distributed, with higher frequencies near 0°, 45°, and 90°. Overall, these findings confirm that ion milling plays a crucial role in enhancing the preferred orientation of α-$CoSn_3$ and thereby improving the control of subsequent Sn grain orientation.

5. Conclusion

In this study, we demonstrated that ion-milled α-$CoSn_3$ can guide the crystallographic orientation of Sn grains. The results can be summarized as follows:

1. A modified edge-to-edge lattice matching model was proposed, accounting for both straight and zigzag atom rows. Among the identified pairs, the (1 0 1) β-Sn/(600) α-$CoSn_3$ configuration showed the lowest d-value mismatch (0.64 %), indicating a favorable nucleation condition owing to minimized interfacial energy.
2. α-$CoSn_3$ IMCs formed at the Sn/Co interface after reflowing at 267 °C exhibited anisotropic growth behavior, with the (600) planes tending to align perpendicular to the substrate surface. Argon ion milling enhanced the exposure of these preferentially oriented grains.
3. EBSD analysis revealed that the Sn grains nucleated on the ion-milled α-$CoSn_3$ surface preferentially aligned their [001] axis within 30° of the substrate. This experimental observation is consistent with the predicted low-energy lattice matching relationship.

In summary, these results provide a practical approach for tailoring Sn grain orientation using polycrystalline Co substrates, thereby avoiding the need for expensive single-crystal seeds. The proposed strategy is promising for improving the performance and longevity of microelectronic solder joints through interfacial crystallographic engineering.

Declaration of Generative AI and AI-assisted technologies in the writing process

During the preparation of this work the author(s) used GPT-4 in order to improve the readability and language of the manuscript. After using this tool/service, the author(s) reviewed and edited the content as needed and take(s) full responsibility for the content of the publication.

CRediT authorship contribution statement

Xinjie Wang: Writing – original draft, Visualization, Software, Methodology, Investigation, Formal analysis, Data curation, Conceptualization. **Hiroaki Tatsumi:** Writing – review & editing, Supervision, Project administration. **Chia-Lin Li:** Methodology, Investigation, Formal analysis. **Jyh-Wei Lee:** Supervision, Methodology, Funding acquisition. **Hiroshi Nishikawa:** Writing – review & editing,

Supervision, Methodology, Funding acquisition.

Declaration of competing interest

The authors declare that they have no known competing financial interests or personal relationships that could have appeared to influence the work reported in this paper.

Acknowledgment

The authors thank the China Scholarship Council (grant number 202206120054) for partial financial support.

Appendix A. Supplementary data

Supplementary data to this article can be found online at https://doi.org/10.1016/j.matdes.2025.115329.

Data availability

Data will be made available on request.

References

[1] Y.-J. Seo, J.-W. Yoon, Effects of solder volume and size on microstructures and mechanical properties of Sn-3.0Ag-0.5Cu solder joints, J. Mater. Sci. Mater. Electron. 33 (2022) 16700–16709, https://doi.org/10.1007/s10854-022-08567-1.
[2] S. Li, X. Wang, M. Liao, Z. Li, Q. Li, H. Yan, A. Liu, F. Wang, Microstructures, mechanical properties and reliability induced from size effect in Sn-based solder joints, J. Mater. Res. Technol. 35 (2025) 5067–5083, https://doi.org/10.1016/j.jmrt.2025.02.169.
[3] M. Abtew, G. Selvaduray, Lead-free solders in microelectronics, Mater. Sci. Eng. R. Rep. 27 (2000) 95–141, https://doi.org/10.1016/S0927-796X(00)00010-3.
[4] L.P. Lehman, Y. Xing, T.R. Bieler, E.J. Cotts, Cyclic twin nucleation in tin-based solder alloys, Acta Mater. 58 (2010) 3546–3556, https://doi.org/10.1016/j.actamat.2010.01.030.
[5] Z.L. Ma, S.A. Belyakov, K. Sweatman, T. Nishimura, T. Nishimura, C.M. Gourlay, Harnessing heterogeneous nucleation to control tin orientations in electronic interconnections, Nat. Commun. 8 (2017) 1916, https://doi.org/10.1038/s41467-017-01727-6.
[6] D.G. House, E.V. Vernon, Determination of the elastic moduli of tin single crystals, and their variation with temperature, Br. J. Appl. Phys. 11 (1960) 254, https://doi.org/10.1088/0508-3443/11/6/308.
[7] V.T. Deshpande, D.B. Sirdeshmukh, Thermal expansion of tin in the β–γ transition region, Acta Crystallogr. 15 (1962) 294–295, https://doi.org/10.1107/S0365110X62000742.
[8] B.F. Dyson, T.R. Anthony, D. Turnbull, Interstitial diffusion of copper in tin, J. Appl. Phys. 38 (1967) 3408, https://doi.org/10.1063/1.1710127.
[9] B.F. Dyson, Diffusion of gold and silver in tin single crystals, J. Appl. Phys. 37 (1966) 2375–2377, https://doi.org/10.1063/1.1708821.
[10] D.C. Yeh, H.B. Huntington, Extreme Fast-Diffusion System: Nickel in Single-Crystal Tin, Phys. Rev. Lett. 53 (1984) 1469–1472, https://doi.org/10.1103/PhysRevLett.53.1469.
[11] Y.-A. Shen, J.A. Wu, Effect of Sn grain orientation on reliability issues of Sn-rich solder joints, Materials 15 (2022) 5086, https://doi.org/10.3390/ma15145086.
[12] P. Zhang, S. Xue, J. Wang, New challenges of miniaturization of electronic devices: Electromigration and thermomigration in lead-free solder joints, Mater. Des. 192 (2020) 108726, https://doi.org/10.1016/j.matdes.2020.108726.
[13] K. Xu, X. Fu, X. Wang, Z. Fu, X. Yang, S. Chen, Y. Shi, Y. Huang, H. Chen, The effect of grain orientation of β-Sn on copper pillar solder joints during electromigration, Materials 15 (2021) 108, https://doi.org/10.3390/ma15010108.
[14] M.N. Bashir, S.U. Butt, M.A. Mansoor, N.B. Khan, S. Bashir, Y.H. Wong, T. Alamro, S.M. Eldin, M. Jameel, Role of crystallographic orientation of β-Sn grain on electromigration failures in lead-free solder joint: an overview, Coatings 12 (2022) 1752, https://doi.org/10.3390/coatings12111752.
[15] T.C. Huang, T.L. Yang, J.H. Ke, C.H. Hsueh, C.R. Kao, Effects of Sn grain orientation on substrate dissolution and intermetallic precipitation in solder joints under electron current stressing, Scr. Mater. 80 (2014) 37–40, https://doi.org/10.1016/j.scriptamat.2014.02.010.
[16] K.-N. Tu, Reliability challenges in 3D IC packaging technology, Microelectron. Reliab. 51 (2011) 517–523, https://doi.org/10.1016/j.microrel.2010.09.031.
[17] Y. Qiao, N. Zhao, Anisotropy-induced reliability issues and grain orientation control in Sn-based micro solder joints for advanced packaging, J. Mater. Sci. Technol. 224 (2025) 267–291, https://doi.org/10.1016/j.jmst.2024.10.044.
[18] Z.L. Ma, J.W. Xian, S.A. Belyakov, C.M. Gourlay, Nucleation and twinning in tin droplet solidification on single crystal intermetallic compounds, Acta Mater. 150 (2018) 281–294, https://doi.org/10.1016/j.actamat.2018.02.047.
[19] Z.L. Ma, C. Li, S.Y. Yang, X.W. Cheng, Controlling βSn grain orientations in electronic interconnects with single-crystal Cobalt substrates, Acta Mater. 194 (2020) 422–436, https://doi.org/10.1016/j.actamat.2020.04.059.
[20] S. Olliges, P. Gruber, A. Bardill, D. Ehrler, H.D. Carstanjen, R. Spolenak, Converting polycrystals into single crystals–selective grain growth by high-energy ion bombardment, Acta Mater. 54 (2006) 5393–5399, https://doi.org/10.1016/j.actamat.2006.07.005.
[21] D. Manova, J.W. Gerlach, S. Mändl, Thin film deposition using energetic ions, Materials 3 (2010) 4109–4141, https://doi.org/10.3390/ma3084109.
[22] Y. Wang, S. Liu, L. Ma, C. Zhen, J. Wang, F. Guo, Optimal thickness of nanocrystalline cobalt-phosphorus coating with good diffusion resistance and small space requirement for solder joints, J. Mater. Res. Technol. 35 (2025) 4848–4858, https://doi.org/10.1016/j.jmrt.2025.02.158.
[23] S. Liu, L. Ma, C. Zhen, Y. Wang, D. Li, F. Guo, Strategies for solder joints with high shear strength, slow interfacial consumption, ductile intermetallic compounds using hybrid crystalline-amorphous Co-P coatings, Mater. Des. 224 (2022) 111385, https://doi.org/10.1016/j.matdes.2022.111385.
[24] S. Liu, L. Ma, C. Zhen, F. Guo, Thermal fatigue behavior of Cu/Co-P/Sn/Co-P/Cu solder joint interface with crystalline/amorphous Co-P coating, in: 2023 24th Int. Conf. Electron. Packag. Technol. ICEPT, IEEE, 2023: pp. 1–4. DOI: 10.1109/ICEPT59018.2023.10492106.
[25] J.-S. Fang, T.-H. Su, Y.-L. Cheng, G.-S. Chen, Synergistic enhancement of adhesion and electromigration reliability of cobalt via super-diluted (0.06 at.%) tungsten alloying as next-generation interconnect materials, Microelectron. Reliab. 158 (2024) 115427, https://doi.org/10.1016/j.microrel.2024.115427.
[26] J.-S. Fang, G.-S. Chen, C.-C. Chang, C.-N. Hsiao, W.-C. Chen, Y.-L. Cheng, Understanding electromigration failure behaviors of narrow cobalt lines and the mechanism of reliability enhancement for extremely dilute alloying of manganese oxide, J. Alloys Compd. 970 (2024) 172591, https://doi.org/10.1016/j.jallcom.2023.172591.
[27] B. Vonnegut, D. Turnbull, Nucleation catalysis, Ind. Eng. Chem. 44 (1952) 1292–1298, https://doi.org/10.1021/ie50510a031.
[28] B.L. Bramfitt, The effect of carbide and nitride additions on the heterogeneous nucleation behavior of liquid iron, Metall. Trans. 1 (1970) 1987–1995, https://doi.org/10.1007/BF02642799.
[29] M. Zhang, P. Kelly, M. Easton, J. Taylor, Crystallographic study of grain refinement in aluminum alloys using the edge-to-edge matching model, Acta Mater. 53 (2005) 1427–1438, https://doi.org/10.1016/j.actamat.2004.11.037.
[30] N. Zhong, X. Wang, Z. Guo, Y. Rong, Orientation Relationships between Ferrite and Cementite by Edge-to-edge Matching Principle, J. Mater. Sci. Technol. 27 (2011) 475–480, https://doi.org/10.1016/S1005-0302(11)60094-7.
[31] H. Swanson, E. Tatge, Standard X-ray diffraction powder patterns. Natl. Bur. Stand. (US) Circ. 539, Volume 1 (1953) 24–26.
[32] A. Lang, W. Jeitschko, Two new phases in the system cobalt-tin: the crystal structures of {alpha}-and {beta}-CoSn {sub 3}, Z. Fuer Met. 87 (1996) 759–764.
[33] M.-X. Zhang, P.M. Kelly, Edge-to-edge matching and its applications: Part I Application to the Simple HCP/BCC System, Acta Mater. 53 (2005) 1073–1084, https://doi.org/10.1016/j.actamat.2004.11.007.
[34] Z.L. Ma, S.A. Belyakov, C.M. Gourlay, Effects of cobalt on the nucleation and grain refinement of Sn-3Ag-0.5 Cu solders, J. Alloys Compd. 682 (2016) 326–337, https://doi.org/10.1016/j.jallcom.2016.04.265.
[35] Z.L. Ma, C.M. Gourlay, Nucleation, grain orientations, and microstructure of Sn-3Ag-0.5 Cu soldered on cobalt substrates, J. Alloys Compd. 706 (2017) 596–608, https://doi.org/10.1016/j.jallcom.2017.02.243.
[36] A. Leineweber, M. Hoppe, S. Martin, C. Schimpf, S.L. Shang, Z.K. Liu, Stacking-disordered CoSn3 and tetragonally stacked CoSn4 formed during solid-state interdiffusion of Co and Sn, Intermetallics 160 (2023) 107957, https://doi.org/10.1016/j.intermet.2023.107957.
[37] R. Becker, W. Döring, Kinetische behandlung der keimbildung in übersättigten dämpfen, Ann. Phys. 416 (1935) 719–752, https://doi.org/10.1002/andp.19354160806.
[38] D. Turnbull, Formation of crystal nuclei in liquid metals, J. Appl. Phys. 21 (1950) 1022–1028, https://doi.org/10.1063/1.1699435.
[39] D. Turnbull, B. Vonnegut, Nucleation Catalysis, Ind. Eng. Chem. 44 (1952) 1292–1298, https://doi.org/10.1021/ie50510a031.